

NASA Technical Memorandum 88800

NASA-TM-88800 19860020734

Feasibility Study of a Discrete Bearing/Roller Drive Rotary Joint for the Space Station

Stuart H. Loewenthal and Fredrick T. Schuller
Lewis Research Center
Cleveland, Ohio

July 1986

LIBRARY COPY

AUG 13 1986

LANGLEY RESEARCH CENTER
LIBRARY, NASA
HAMPTON, VIRGINIA

NASA

Trade names or manufacturers' names are used in this report for identification only. This usage does not constitute an official endorsement, either expressed or implied, by the National Aeronautics and Space Administration.

FEASIBILITY STUDY OF A DISCRETE BEARING/ROLLER
DRIVE ROTARY JOINT FOR THE SPACE STATION

Stuart H. Loewenthal and Fredrick T. Schuller
National Aeronautics and Space Administration
Lewis Research Center
Cleveland, Ohio 44135

SUMMARY

Perhaps the most critical mechanism on board the proposed space station is the continuously rotating joint which must accurately align the solar power units with the sun during earth orbit. The feasibility of a multiple, discrete bearing supported joint driven by a self-loading, "pinch" roller drive actuator was investigated for this application. This concept appears to offer greater protection against catastrophic jamming, less sensitivity to adverse thermal gradients, greater accessibility to inorbit servicing or replacement and greater adaptability to very large (5 m) truss members than to more conventional continuous support bearing/gear reducer joints. Analytical trade studies performed herein establish that a discrete cam roller bearing support system having eight hangers around a continuous ring would provide sufficient radial and bending stiffness to prevent any degradation in the fundamental frequencies of the solar wing structure. Furthermore, it appears that the pinch roller drive mechanism can be readily sized to meet or exceed system performance and service life requirements. Wear life estimates based on experimental data for a steel roller coated with an advanced polyimide film show a continuous service life more than two orders of magnitude greater than required for this application.

INTRODUCTION

A gravity gradient stabilized, power tower was initially established as the reference configuration for the space station (ref. 1). More recently, a "twin keel" version, similar to that shown in figure 1 but with solar heat collectors replacing the outboard solar panels, has been selected for further development. This later configuration locates the habitation and laboratory modules near the station's center of gravity in order to reduce microgravity levels. Both configurations require that the solar power conversion units or receivers track the sun at the approximate orbit rate of 1 revolution per 94 min. Perhaps the most critical mechanism on board the station will be the rotary joint which performs this tracking function. It must position the solar receivers to within about $\pm 1^\circ$ normal to the sun in the case of a photovoltaic receiver and to about $\pm 0.1^\circ$ for the solar dynamic collector (solar heat engine) for acceptable conversion efficiency. Thus a highly accurate drive system will be needed for the "hybrid" system now under study. Part of the solar energy captured during the sunlit portion of the orbit will be stored by the station's batteries or fuel cells for later use during the period of about 39 min when the station is in the earth's shadow.

Due to the large inertia of the solar receivers and the long length of the transverse booms, structural stiffness across this so called "alpha" joint must be maximized in order to reduce deflection and accelerations as well as

E-3138

N86-30206 #

maximize actuator response rate. The joint must contain a rotary means to transfer electrical power and data signal across the rotating interface. Furthermore, the rotary drive mechanism itself must provide smooth motion, have long life in a space environment and have inherent fail-safe characteristics. Additional requirements such as serviceability, damping characteristics, physical size, and cost also enter into consideration.

The size of the alpha joint has not yet been established. Initial studies concentrated on a joint about 2.4 m (8 ft) in diameter for the reference configuration's 2.7 m (9 ft) truss section. However, the alpha joint will probably be larger now that a 5 m (16.4 ft) section, erectable structure has recently been selected. Two alpha joints will be needed, one on each side of the transverse boom to drive the outboard rotating solar wings. The joint's support bearings must be structurally integrated into the truss structure in such a way that the joint's effective stiffness is at least as high as the parent truss structure. Otherwise the fundamental frequencies of the system will be degraded.

In addition to the alpha joints, two other types of rotating joints will be required. A "beta" joint, mounted on each solar receiver axis, at right angles to the transverse boom, will oscillate the receivers through $\pm 52^\circ$ to correct for seasonal variations and nodal regression of the orbit. Another rotary joint will also be required to position the thermal radiator panels at a right angle to the sun in order to maximize the radiative cooling rate. This joint will be either continuously rotating at the orbit rate or oscillating back and forth depending on whether a rotating thermal fluid seal or coilable fluid hose will be used.

The structural truss trade study performed in reference 2 concluded that a 4.6 m (15 ft) truss is preferred in terms of growth capability and payload accommodation. This study also indicated that a continuous bearing for a rotary joint for a structure this size may require extensive development. As an alternative, an alpha joint concept was presented in reference 2 which utilizes multiple discrete bearing hangers mounted against a continuous annular ring. A subsequent parametric analysis of this joint concept performed in reference 3, established the basic structural feasibility of this configuration together with minimum bearing and drive stiffness values required to maintain the fundamental vibration frequencies of the truss structure.

This discrete bearing approach of references 2 and 3 is conceptually similar to that proposed earlier in a novel joint concept appearing in reference 4. This rotary joint concept used individual caster bearing assemblies to support an annular channel, connected to the rotating solar wings. A roller actuator system, in traction contact with the ring, turned the joint not unlike a ferris wheel. The roller drive is virtually unjammable and permits positioning of the solar receivers with accuracies in the arc-minute range. The technology associated with roller drives for servo positioning applications is extensively discussed in reference 5.

The objective of this current investigation is to extend and refine the roller drive concept of reference 4, embodying the essential structural features of references 2 and 3. The ability of the proposed joint concept to meet operational stiffness, reliability, and life requirements will be assessed. Material considerations, bearing characteristics and torque requirements will also be addressed.

BACKGROUND ON TRACTION DRIVES

Adjustable speed traction drives have been in commercial service for more than 50 yr, performing a speed regulation function for a wide range of industrial machinery (ref. 6). Speed regulation accuracies typically range from about ± 1 percent with open loop control to about ± 0.1 percent with feedback control or with open loop control when the loads are relatively constant.

Due to their smooth torque transfer characteristics, low rolling friction and undetectable backlash, traction actuators appear to be suitable for aerospace servo mechanisms. One example is the constant speed generator traction drives that have been in service on several commercial and military aircraft such as on the AV8-A Harrier VSTOL fighter. Also "pinched" roller drive systems similar to those commonly used in printing and paper handling machinery have been incorporated in some spacecraft deployment mechanisms. Space vehicle applications include a pinch roller drive mechanism for deploying a spool-wrapped antenna for the Helios B satellite and one that dispenses and stores a transfer boom for Skylab (ref. 5).

Torque capacity and torque-to-weight ratios of well designed traction drives are quite competitive with the best gear transmissions. An experimental, light-weight helicopter transmission which incorporate steel traction rollers lubricated with synthetic traction fluids has been tested at the authors' laboratory at power levels to 370 kW (ref. 6). This is more than 50 percent higher than the power rating of the production gear transmission which was used to set design specifications. Other tests performed on a 50 000 rpm, automotive gas turbine roller drive and on a 70 000 rpm, cryogenic boost pump roller drive operated in LOX clearly establish the ability of traction drives to meet very demanding performance requirements (ref. 6).

Servo-Actuator Characteristics

Since servo motors are generally high speed, low torque devices, it is usually necessary to introduce a mechanical speed reducer between the motor and the load. However, this reducer must have certain performance characteristics if the operational quality of the system is to be maintained. These are discussed as follows:

Zero backlash. - Because traction contacts are in continuous engagement, they exhibit no backlash discontinuity or "deadband" upon torque or direction reversals. This is very desirable for tracking type mechanisms where deadband nonlinearities are difficult to contend with from a servo control viewpoint. However, due to tangential inelastic displacements under torque, some hysteresis displacements will occur. This precludes the use of roller drives from precision, point-to-point positioning applications, unless a closed-loop control is used.

High torsional stiffness. - For maximum response (minimum response time) for point-to-point motion control, it is desirable to maximize drive system torque-to-inertia ratios and system torsional stiffness. Traction contacts tend to be several times stiffer than gears due to the absence of tooth bending deflections (ref. 5).

Low torque ripple and velocity errors. - Perturbations and errors in motion transmission can upset sensitive instruments such as optical scan systems and also contribute to control system instabilities. Transmission by precision rollers is inherently smooth, while some amount of cogging is unavoidable with even the highest quality gears due to tooth kinematic errors and load transfer from tooth to tooth.

Precise resolution. - High resolution capability as well as positional accuracy are among the most critical factors for judging the performance of a servo mechanism. Repeatability is another important factor. Nearly infinite speed and ratio adjustment is possible for adjustable traction drives limited only by the capabilities of the servo-control system. For example, a traction roller feed drive system developed by Lawrence Livermore Laboratory for an ultra-precision turning machine (ref. 7) has a linear resolution capability of 5 nm (0.2 μ in.), equivalent to 0.05 arc sec of rotation.

Dry operation - The roller contact due to its low sliding nature can take advantage of dry film lubrication for extended periods of time under low to moderate power conditions. This can be accomplished by either using high traction solid film coatings such as ion-plated gold or silver or using advanced, low-wear polymers such as partially fluorinated polyimides or polyamide-imides. This is vividly illustrated by tests of a 120:1 ratio, 5 kW planetary traction drive which ran fully preloaded for 43 hr at 360 000 rpm without failure using no liquid lubrication whatsoever (ref. 6). Such speeds are difficult to sustain even with well designed, oil lubricated gears. The elimination of a depletable liquid lubrication is a decided benefit for most spacecraft mechanism applications.

Nonjamming. - Rollers, unlike gears, have the ability to harmlessly slip at predetermined traction limits. The over torque, release-clutch-tendency can prevent catastrophic damage if jamming should occur at some point in the mechanism drivetrain.

Synchronization free - In the case of dual fault or multiple redundant servo drive mechanisms, such as those for some spacecraft applications, independent, multiple drive rollers can be readily engaged and disengaged from drive systems with conventional linear actuators without the need to stop the system from rotating or the need to provide proper tooth mesh phasing.

ALPHA JOINT OPERATING REQUIREMENTS

Table I lists the operating design requirements for the alpha rotary joint analyzed in this study. Most of the parameters listed except as noted are based on the Space Station Initial Operating Capability (IOC) reference configuration from reference 1. A maximum acceleration rate of 0.003°/sec² was selected to allow the joint to regain nominal operating speed within 30 sec from rest in the event of a shutdown while in orbit. This acceleration rate would also enable a stationary solar wing to reregister itself with the other wing inside of 370 sec under the worst case without exceeding the 0.5°/sec maximum slew rate.

Maximum transient loads acting on the joint occur during the orbiter locking maneuver. These loads, appearing in table I, were computed in reference 1

from the transient response due to a 2224 N (500 lb) step load for 1 sec duration at the docking port. Torsional and bending stiffness values (from ref. 8) for the joint are based on preserving the stiffness of a 2.7 m (9 ft) box truss structure made from graphite epoxy tubing.

In addition to the 10 yr unattended life requirement, the joint should provide fail safe operation without causing failure of additional components. Redundant functional paths are to be incorporated. The joint should also permit on-orbit scheduled maintenance without interruption of other critical-services.

Finally, no backlash in the drive actuator path and no "play" in the joint support bearings will be permitted.

ROLLER/WHEEL ROTARY JOINT CONCEPT

The first alpha joint concept that was investigated is shown in figures 2 and 3. A spring loaded, linear actuator engages and loads a traction drive roller against the inside diameter of an annular wheel having radial spokes. The drive roller is driven at a rotational speed of approximately 19 rpm by a brushless, dc torque motor having a nominal peak power rating of 22 W. This power level is double that actually required for rotation under peak loading in order to provide a two times safety margin.

The annular wheel is radially supported by the outer race bearings of a 100:1 ratio harmonic speed reducer as shown in figure 4. The harmonic drive is a relatively well known speed reducing mechanism that has flown on a number of spacecraft including Pegos and Skylab. More recently, NASA JPL has incorporated two doubly redundant harmonic drives in the Galileo spacecraft antenna deployment actuator. The output of the harmonic drive is used to drive the rotating solar wing at the required nominal rotor speed of $0.064^\circ/\text{sec}$ (1 revolution per 94 min).

Bending moment loads are reacted by a set of caster bearing rollers (fig. 5 shows three sets) which are equally positioned around the perimeter of an annular channel that is integral with the transition truss structure. The caster assembly consists of two individual rollers that are spring loaded in opposite directions against opposing faces of the annular ring. The spring preload is selected to match the required bending stiffness of the parent structure. The number of caster sets and spring stiffness values can, of course, be varied to best meet the needed frequency response of the structure. Active/passive damping and stiffness control via a servo actuator can be conveniently incorporated if such added complexity is warranted.

DIRECT ROLLER DRIVE ROTARY JOINT CONCEPT

In the interest of simplifying the previous rotary joint arrangement, an improved design was investigated. In this second version, a "pinch" roller actuator is in direct driving contact against the rotating support ring as illustrated in figure 6. This eliminates the harmonic drive with its intermediate rotating support structure and allows additional room within the interior of the joint for the installation and servicing of the electrical power/data transfer unit. In addition, one or more active and redundant slave

drive modules can be conveniently interspersed between the discrete bearing hangers of the alpha joint concept evaluated in references 2 and 3. In this way the rotating support ring which is used as the guide member for the bearing rollers serves double duty as the driven track member for the roller drive. Thus a separate internal or external ring gear, required for a gear drive unit, is not needed.

Pinch Roller Drive

A conceptual sketch of the "pinch" roller drive module appears in figure 7. Pinch roller drives are common feed regulating mechanisms for paper and film handling equipment, such as printing and copying machines as well as computer plotting devices. In these applications, the processed material is normally "pinched" between elastomer-coated drive rollers. The high accuracy required for registering the paper in multicolor printing operations and for computer plotting devices can readily be met. With steel rollers positional resolution of 0.2 nm (0.2 μ in.) have been demonstrated in the precision machine tool feed system (ref. 7) described earlier. Pinch roller drive mechanisms have also been used in space. This type of drive was used for deploying a flat-wrapped antenna from a spool in the Helios B satellite (ref. 9). In another application, a pinch drive dispensed and retrieved a flat-wrapped transfer boom for Skylab (ref. 10). In addition, polyurethane-coated roller actuators have been successfully used in dry rolling contact on military spacecraft.

It is envisioned that one active and one or more "backup" pinch roller drive modules, like that shown in figure 7, would be interspersed between the bearing hangers around the support ring. These units could be easily engaged or disengaged with the joint rotating by simple linear solenoid actuators as shown in figure 7. These modules would be connected on stiff tubular support struts similar to those supporting the bearing hangers. However, it would be desirable to purposely introduce some greater amount of radial compliance in the drive mounts to accommodate some degree of guide track runout. By pinching the guide track between the two drive rollers, the roller's normal load (not to exceed 445 N or 100 lb) would cause negligible bending distortion to the relatively thin annular guide track.

Each of the drive rollers are powered by dc torque motors that are individually mounted to the stationary frame member through flexural pivots. These commercially available flexural pivots have virtually negligible hysteresis. Radial load capacities are available up to 8 000 N (1800 lb) for a nominal 25 mm diameter pivot. The pivot would be pre-wound by a few degrees at start of engagement to provide an initial contact preload that was 10 to 15 percent of the nominal operating value. This would ensure proper traction engagement at start up.

Self-loading drive. - When the drive motors are energized a traction force is generated between the drive rollers and supporting ring. Due to the pivoting action of the drive motor assembly, the traction force will tend to wedge the rollers against the ring, thereby generating a normal force P . The induced normal force P is related to the traction force F_t through the expression:

$$P = F_t \left(\frac{1}{\tan \theta} + \frac{r}{(c) \sin \theta} \right)$$

Where θ , r and c are geometric parameters illustrated in figure 8. Since the design traction coefficient $\mu = F_t/P$, it follows that μ can be readily set by selecting the appropriate geometric parameters θ , r and c from the following:

$$\mu = \frac{\sin \theta}{\left(\cos \theta + \frac{r}{c} \right)}$$

For example, if $r = 50$ mm and $c = 75$ mm, then a $\theta = 19^\circ$ will produce a $\mu = 0.2$, and a $\theta = 28^\circ$ yields a $\mu = 0.3$ and so on. The design traction coefficient is normally selected to be 70 to 80 percent of the maximum traction coefficient of the contact at the point of gross slip. This 20 to 30 percent margin is to ensure that no slip will occur under the most adverse condition. The maximum traction coefficient at slip is a function of the material and geometry of the contact as well as the operating conditions, viz. speed, contact pressure and temperature. It is normally determined experimentally under the conditions of interest. Roller material considerations and design will be addressed later in this report.

Travel limit pin. - As load is applied across the contact, small structural deformation will occur which will decrease design θ causing P to increase and in turn reducing design μ . Normally, structural deflection will be small, on the order of fractions of a millimeter, and the change in μ would be only a couple of percent. A travel limit pin such as that shown in figure 7 could arrest motion of the loading lever at some predetermined amount of travel, thereby preventing a further increase in contact normal load. At this point additional torque loading would drive the traction force, hence traction coefficient, up until the slip traction coefficient was reached. Any additional torque loading would then cause the drive roller to slide over the ring, limiting the maximum torque that could be reacted by the drive assembly. This "over torque" clutch action would prevent harmful damage to the drive mechanism and structure during transient overloads or in the event of bearing jamming. This over torque slip characteristic is viewed as a distinct advantage over gear drive mechanism which could permit significant damage to the structure in the event of a jam or shock load.

CAM BEARING SUPPORT SYSTEM

A prime design objective of the alpha joint transition structure and support bearing system is to preserve the stiffness of the parent solar wing structure. Otherwise the increased bending and torsional natural frequencies attained by the relative stiff solar wing box structure will be sacrificed. A traditional approach to the support bearing system problem is to incorporate a pair of preloaded, thin-section ball bearings or a single preloaded thin section, four-point-contact bearing. These thin-section bearings have small (25 to 50 mm) cross sections relative to their diameters, helping to reduce their weight.

Four-point, thin-section ball bearings, having gothic arch inner and outer races, have flown on several satellites. This type of bearing can be

obtained in bore sizes to about 122 cm (48 in.). In larger sizes "wire race" bearings are available. These have been used on missile launchers, tank turrets and radar systems. The largest wire race bearing ever used in space was a 1.8 m (6 ft) bearing for a rotating pallet in the STS payload bay.

In the proposed application, a significantly larger continuous bearing, on the order of 2.4 to 4.3 m (8 to 14 ft) will be needed. Because of the flexibility of these large bearing's thin cross section and because it will be mounted in a semi-flexible structure, it will be difficult to maintain a uniform preload around the bearing. The preload must be relatively large to keep joint stiffness high, so bearing drag torque will be sensitive to out-of-plane distortions.

Furthermore, thermal gradients across a large, thin-section bearing can also cause large variations in drag torque, as the bearing slowly rotates from the sun side to the shade side. For example, torque tests on relatively small 177 mm bore, four-point contact bearings reported in reference 11 showed a 3 to 5 times increase in operating torque when the inner race temperature was 10 °C higher than that of the outer race. This temperature sensitivity will be amplified for larger bearings since the increase in interference would be proportional to bearing size. For example, just a 1 °C increase in temperature of the inner race relative to the outer race will cause a diametral interference of 0.059 mm (0.0023 in.) on a 2.7 m (108 in.) bore bearing having aluminum races. It is not difficult to imagine that only a few degrees in temperature difference could jam such a bearing that has already been heavily preloaded to maintain joint stiffness. Furthermore, it is likely that the bearing will not remain round due to the high radial thermal gradient that is imposed from its sun side across to its shade side. Techniques to minimize thermal gradients, such as insulation and heaters will be essential to stabilize operating torque levels, provided such a technique is feasible at all. In addition, lubrication and sealing very large bearings for long space life are also concerns. The large size also hampers maintenance and eliminates insitu replacement procedures. Manufacturing capabilities to make continuous rather than segmented inner and out races is yet another concern for bearings in excess of 2.7 m.

An alternative to a very large, "continuous" bearing, is to mount a number of individual caster or cam roller type bearings around the joint as shown in figure 6. In this way, bearing preload control, thermal gradient problems, lubrication, and sealing problems have been largely overcome. Also EVA replacement or servicing of an individual bearing assembly can be readily accomplished. Furthermore, the single-point failure mode of a one bearing joint can be eliminated and problems associated with manufacturing extremely large bearings are no longer an issue.

Figure 9 illustrates one possible configuration in which the rotating annular support ring is trapped in three-point contact by a set of sealed cam roller bearings. An easily adjusted preload washer will set and maintain a predetermined bearing load, hence drag torque and stiffness, independent of minor structural deflections and thermal gradients. On orbit replacement of individual bearings can be readily accomplished with special bearing mounts.

Figure 10 shows an alternate arrangement where the moment support function and the shear support function have been decoupled. Here radially oriented cam bearings take joint moment loads but allow ring runout and thermal growth while

the relatively small shear loads are carried by a roller bearing which circumscribes the dual roll ring assembly.

Bearing Support Stiffness

Required bending and torsional stiffness of the alpha joint from reference 8 appears in table I. The bending stiffness (M/γ) is related to the axial bearing support stiffness K_A at each of the eight bearing hangers according to the following relation, equation (A-5) derived in appendix A:

$$K_A = \frac{M}{\gamma} \frac{1}{4R^2}$$

For rotating support rings with diameters of 2.4 and 4.3 m (8 and 14 ft) $K_A = 8.9 \times 10^7$ N/m (5.1×10^5 lb/in.) and 2.9×10^7 N/m (1.7×10^5 lb/in.) respectively, for the joint bending stiffness value appearing in table I.

A finite element analysis was used in reference 3 to predict the effect of bearing support axial and radial stiffness on the first bending and first torsional frequencies of the solar wing. According to figure 11, taken from reference 3, axial stiffness values above about 1.8×10^7 to 1.8×10^8 N/m (10^5 to 10^6 lb/in.) or radial stiffness values above about 1.8×10^7 N/m (10^5 lb/in.) will not cause an appreciable decay in the solar wing's fundamental bending or torsional frequencies for either joint diameter. This basically agrees with the axial stiffness values derived above from the required bending stiffness of 5.31×10^8 N-m/rad listed in table I.

Bending and radial stiffnesses for the proposed cam bearing system were calculated in appendix B. They appear as a function of preload and joint diameter in table B-4. At a bearing preload of 445 N, the system bending stiffness was at least 34 times greater than that required for either steel rollers against a steel ring or against an aluminum ring. Similarly, radial stiffness values were a minimum of 87 times that required to preserve the fundamental solar wing frequencies. As shown in appendix B, a minimum bearing preload of 742 N would be required to react the transient shuttle berthing moment of 4220 N-m (see table I) without unseating the cam bearing/ring contact. Bearing preload has only a modest effect on stiffness as shown in table B-4.

Transition Truss

The cam bearing system stiffness calculated in appendix B does not account for the stiffness characteristics of the transition truss. Figure 6 shows one possible transition truss configuration. The bending and torsional stiffness of the parent 2.74 m (9 ft) truss, made from carbon-graphite epoxy tubes, is 5.42×10^8 and 1.32×10^8 m-N-m divided by meters of length, respectively according to reference 1. If the joint occupies one unit cell of 2.74 m in length, then the effective stiffness of the transition trusses K_{TT} in combination with cam bearing stiffness K_B should not be less than the parent truss bending stiffness of 1.98×10^8 N-m/rad.

As an example, figure 12 shows a NASTRAN model of the proposed transition truss structure. This structure is comprised of 63.5 mm (2.5 in.) diameter, 4.76 mm (0.19 in.) wall thickness carbon-graphite tubing having an elastic modulus of 276 GPa (40×10^6 psi). This structure has a bending stiffness of 4.6×10^9 N-m/rad, for pinned bearing hanger connections, fixed truss connections and, when the bearing hangers are constrained, to lie in a plane under the imposed bending moment. Considering that the left transition truss, bearing support system and the right transition truss act like three springs in series, the effective bending stiffness of the joint is 2.04×10^9 N-m/rad. This compares favorably with the parent truss bending stiffness cited above, even though the model does not take credit for the additional stiffness that will be provided by the circular ring track structure.

ROLLER ACTUATOR DESIGN

The pinch roller drive system as shown in figure 7 must produce sufficient traction to overcome drag torque associated with the support bearings and electrical power/signal transfer device as well as the torque needed to accelerate the solar wing up to speed in a reasonable amount of time. Based upon the analysis contained in appendix C, a torque of 31.4 N-m is required to accelerate the four 9.2 by 24 m photovoltaic panels from rest to nominal operating speed in about 21 sec. This cam support bearing torque for eight sets of three bearings each at the required preload found in appendix B was estimated to be 57.6 and 51.6 N-m for the 2.4 and 4.3 m joints, respectively. The roll ring electrical transfer device has an expected drag torque of less than 1 N-m.

The total required output torque was calculated in appendix C to be 166.6 and 153.4 N-m for the 2.4 and 4.3 m. diameter joints, respectively. This estimate is based upon the aforementioned torques, allowing for a 10-percent torque loss in the drive roller/ring contact and then doubling the combined drag torque of all rotating elements to provide a two times safety margin on drive torque, see equation (C-4). This represents a peak drive power of less than 1 W at the nominal rotation rate of $0.064^\circ/\text{sec}$.

A parametric study was conducted in appendix C to determine the best compromise between drive roller size and roller loading conditions. The influence of joint diameter, the design traction coefficient and choice of ring/roller materials on roller contact stresses, normal and unit normal loading was investigated. The roller width to diameter ratio was arbitrarily set equal to 1.5 as a compromise between the possible ill effects of misalignment and the benefits of reduced unit loading.

The results of this trade study are tabulated in table C-1 and appear in figure 13. The benefits of increasing joint diameter in terms of reduced loading is clear from figure 13(a) where the normal load of the 4.3 m joint is about half of the 2.4 m joint. While increasing the design traction coefficient will obviously reduce normal loading, it appears that there is not much incentive to operate with a traction coefficient much above 0.2. Figure 13(b) shows that unit loading diminishes with an increase in roller diameter, as expected, but a roller diameter between 70 and 80 mm seems to be a reasonable compromise.

The choice of ring and roller material combination can obviously have a significant effect on the operating traction coefficient contact stresses, and most importantly service life. Figure 13(c) reflects both the importance of ring/roller material combination and joint size on maximum Hertz stress. Larger joint size is again beneficial, but less so, on an absolute basis for the softer aluminum ring/polymer roller combination. Contact stresses at a given joint size and traction coefficient are reduced by about 25 percent for a steel roller against an aluminum ring relative to a steel ring combination and by about 84 percent for the polymer roller against aluminum. This is due to the lower elastic modulus associated with the aluminum and the polymer relative to steel, which results in a larger contact area at a given normal load. The benefits of low operating contact stress as shown with the polymer roller are not lost if the roller was made of steel but simply coated by the polymer. For example, coating a steel roller with a relatively thin, 25 to 50 μm (0.001 to 0.002 in.) layer of polymer would only increase the contact stress by approximately 5 percent relative to a solid polymer roller according to the analysis of reference 13.

Material Selection Considerations

The choice of the roller/ring material combination is governed primarily by durability characteristics and traction performance in the low earth space operating environment. In the case of traction drives, material combinations which offer the combination of high friction (traction) and low wear rates, not unlike brake materials, are preferred. Space compatibility is another important dictate. In this respect materials and lubrication processes that have been explored or used for spacecraft gears, bearings, and sliding mechanisms are possible candidates. A comprehensive, although not particularly up to date, survey of material for spacecraft lubrication applications can be found in reference 14. These include solid film lubricants such as Au, Ag, MoS_2 and PTFE as well as surface or through hardened metals such as stainless steel and aluminum. Ion-plated gold films appear to have sufficient integrity and traction, when used on an experimental gyro gimbal roller drive (see ref. 15) to warrant further study.

A source of useful data comes from materials that are suitable for spacecraft gearing. A relatively thorough investigation of the tribological performance of many candidate gear materials at a vacuum of 10^{-7} Torr was carried out in reference 16. For medium or heavy loads, plasma-nitrided steel gears were found to give very low wear rates without additional lubrication. For example, a total pinion tooth flank wear depth of about 0.068 mm (0.0027 in.) was measured after about 4×10^7 pinion revolutions under a Hertzian contact stress of 350 MPa (51 000 psi) running completely dry. As a point of comparison, a 76 mm diameter steel roller driving a 2.4 m ring roller would operate under a maximum Hertz stress of just 55 MPa (8 000 psi) at a traction coefficient of 0.2 according to table C-1. At the wear rate found from the higher stress gear tests of reference 16, a nitrided steel drive roller would only wear about 0.003 mm (1.2×10^{-4} in.) deep after 10 yr of running (1.8×10^6 r/s). This estimate is extremely conservative since the roller is actually operating at a contact stress six times less than the gear and with a slide-to-roll ratio that is one to two orders of magnitude smaller.

Reference 16 also established that polyimide plastic gears running against anodized aluminum alloy or stainless steel gear pairs also gave excellent wear rate results although not quite as good as the nitrided steel gear pairs. The best results were obtained with a commercially manufactured polyimide material filled with 15 percent MoS₂.

Self-lubricating polymers such as polyimides (Vespe¹) or polyamide-imides (Torlon¹) are promising candidates for this application due to their dry low wear rates and their relatively high friction (>0.3) in their pure resin or unfilled condition. Furthermore, both resins show excellent compatibility with space environment, having low out-gassing rates, high tolerance to ultra-violet radiation and a relatively low hygroscopic nature relative to other polymers. Both of these materials, polyimide in the form of "Kapton" protective film insulation and polyamide-imide as fasteners for thermal insulation on the space shuttle, have been used in space service. However, both materials, as with many other hydrocarbons, would probably experience some erosion if exposed to a direct flux field of atomic oxygen so some shielding would be required for extremely long space exposure.

The polyamide-imide resin showed outstanding tribological performance in roller traction and capacity tests conducted in reference 17. A 50 mm (2 in.) diameter polyamide-imide roller with a width of 5 mm (0.2 in.) against a steel roller carried a steady radial load of 220 N/mm (49.5 lb/in.) while running in air at a surface velocity of 20 m/sec without any signs of surface distress. The range of measured traction coefficient was 0.25 to 0.35. This represents a minimum steady state power throughout of 5.7 kW. Its vacuum performance, which will undoubtedly be less spectacular due to thermal heating, remains to be determined.

Reference 18 discussed the performance of some experimental (pyromellitic acid dianhydride) of partially fluorinated polyimides, that have exceptionally low wear but high friction. These pin on disks tests conducted with a solid polyimide pin against a metal (Haynes 6B cobalt alloy) disk in air gave friction coefficients of up to twice (>0.8) that of commercial polyimides without any loss in wear.

Recent but as yet unpublished vacuum tests of the pure, experimental polyimide resin conducted by Fusaro (ref. 19) showed it to have similar performance in a vacuum as it does in air. Friction and wear data from this study (ref. 19) of a 440-C stainless steel pin against a steel disk coated with a 25 to 50 mm film of this material appears in figure 14. It appears that the vacuum has had only minor effect on this polyimide, although the other polyimides containing a BT dianhydride showed both lower friction and wear in a vacuum than in air. Figure 13 shows that the experimental film has a steady traction coefficient of about 0.4.

Wear rate. - It is instructive to estimate the service life of a steel drive roller for the alpha joint coated with 50 μm (0.002 in.) of this experimental polyimide film. For this example, a drive roller 76 mm in diameter and 133 mm wide running against a 2.4 m anodized aluminum ring will be selected.

¹Registered tradenames.

The maximum contact stress for this combination is about 7.1 MPa at a traction coefficient of 0.2. This operating traction coefficient leaves about a 100 percent safety margin against slip relative to the measured data appearing in figure 14. The experimental wear rate for this film is $650 \times 10^{-15} \text{ m}^3/\text{m}$ of sliding from the pin-on-disk tests at a computed contact stress of approximately 90 MPa. This wear rate will be assumed for the calculation even though it is likely that the wear rate in the alpha joint application would be substantially less due to the significantly lower contact stress than that used in the experiments.

The wear rate is given in terms of sliding distance,

where:

$$\text{Sliding Dist} = \text{Wear Vol}/\text{Wear Rate}$$

For a 76 mm diameter, 113 mm wide roller, coated with 50 μm of a polyimide film:

$$\text{Wear Vol} = \pi(76 \times 10^{-3}) (113 \times 10^{-3}) (50 \times 10^{-6}) = 1.35 \times 10^{-6} \text{ m}^3$$

Therefore,

$$\begin{aligned} \text{Sliding Dist} &= (1.35 \times 10^{-6} \text{ m}^3) / (650 \times 10^{-15} \text{ m}^3/\text{m}) \\ &= 2.1 \times 10^6 \text{ m} \end{aligned}$$

Since the 76 mm diameter drive roller makes

17 7000 revolutions per yr (2400 mm/76 mm by 1 rev/94 min by 60 min/hr by 24 hr/day by 365 day/1 yr), it follows that the yearly sliding distance, assuming a conservative 1 percent slide-to-roll ratio would be

$$\begin{aligned} \text{Sliding Dist/yr} &= \pi(0.076) (0.01) (177 \text{ 000 revolutions per yr}) \\ &= 422 \text{ m/yr} \end{aligned}$$

Therefore, to wear through the 50 μm in polyimide film coating would take over 4900 yr ($2.1 \times 10^6 \text{ m} / (422 \text{ m/yr})$) of continuous running! Even if the actual wear rate was 300 times higher, the drive roller pair would provide at least 16 yr of continuous service.

CONCLUSIONS

The feasibility of a multiple discrete bearing supported alpha joint, driven by a self loading, "pinch" roller drive actuator was investigated for the space station. The roller drive mechanism offers several performance advantages relative to gears for this application. These include over-torque or jam protection, inherent acceptability to dry or self-lubricating materials, and ease of manufacture, assembly and in situ maintenance. The discrete cam bearing support arrangement is much less sensitive to thermal gradients than a single continuous rolling-element bearing. Furthermore, it is not subject to a single point failure mode, and, unlike a continuous bearing, is virtually joint size unlimited. This last attribute is particularly important for a

station having truss members of 5 m in cross section, or greater, due to the manufacturability concerns of continuous "thin line" bearings above about 2.7 m (108 in.). An analytical investigation was conducted of the structural stiffness characteristics of the discrete bearing support system for joints of 2.4 and 4.3 m in diameter. In addition, performance and durability characteristics of the roller drive actuator were evaluated. The following key findings resulted from this study:

(1) The proposed discrete bearing/roller drive joint design satisfies the expected design operating requirements for the space station alpha-joint.

(2) Bending and radial stiffness values for the proposed design consisting of eight cam-bearing hangers were at least 34 and 87 times greater, respectively, than that required to preserve the fundamental frequencies of the solar wing structure.

(3) A 76-mm diameter drive roller coated with 50 μm of an advanced polyimide film running against an aluminum ring provides an estimated wear life more than two orders of magnitude greater than that required for 10 yr continuous operation based on vacuum, wear test data. Under vacuum test conditions, this polyimide film produces a traction coefficient of 0.4, approximately twice that needed for this particular application.

(4) Increasing drive roller diameter and operating traction coefficient will reduce the required roller unit loading, but this benefit becomes relatively small above a roller diameter of about 75 mm and a traction coefficient of about 0.2.

ACKNOWLEDGEMENT

The authors wish to thank Mr. John Caruso for his diligent efforts in preparing the NASTRAN model of the transition truss structure.

APPENDIX A - BEARING SUPPORT STIFFNESS

Stiffness of the alpha joint should be at least as great as the parent truss structure in order to maintain a relatively high bending and torsional vibration frequency of the solar wing. As the solar wing rotates, the axis of bending will vary with rotation angle, θ , relative to the fixed bearing mounts as shown in figure 6. It is important to determine if during this rotation the linear and radial stiffness of the bearing mount will cause a variation in the bending or radial stiffness in the joint itself.

Bending Stiffness

Consider the simplified joint loading diagram for eight bearing hangers shown in figure 15. If a moment, M , is imposed on the joint, equilibrium requires that

$$\Sigma M = 0$$

$$F_1 X_1 + F_2 X_2 + \dots + F_8 X_8 = M \quad (A-1)$$

where

$$X_1 = R \sin \theta$$

$$X_2 = R \sin (\theta + 45)$$

$$X_3 = R \sin (\theta + 90) = R \cos \theta$$

$$X_4 = R \sin (45 - \theta) = R \cos (\theta + 45) \quad (A-2)$$

$$X_5 = -R \sin \theta$$

$$X_6 = -R \sin (\theta + 45)$$

$$X_7 = -R \sin (\theta + 90) = R \cos \theta$$

$$X_8 = -R \sin (45 - \theta) = R \cos (\theta + 45)$$

If the axial displacements at each bearing hanger are Δ_1 , then the corresponding forces F_1 are

$$F_1 = k_1 \Delta_1$$

$$F_2 = k_2 \Delta_2$$

$$F_3 = k_3 \Delta_3$$

$$F_4 = k_4 \Delta_4 \quad (A-3)$$

$$F_5 = k_5 \Delta_5$$

$$F_6 = k_6 \Delta_6$$

$$F_7 = k_7 \Delta_7$$

$$F_8 = k_8 \Delta_8$$

where $k_1 \rightarrow k_8$ are bearing hanger linear or axial stiffnesses and where $\Delta_1 = X_1\gamma$, $\Delta_2 = X_2\gamma$, $\Delta_3 = X_3\gamma$, etc. Since the bearing hangers are all the same, then their axial stiffnesses are equal, so $k_1 = k_2 = k_3 = \dots k_8 = k_A$ and from equation (A-3)

$$\begin{aligned}
 F_1 &= k_A \gamma X_1 \\
 F_2 &= k_A \gamma X_2 \\
 F_3 &= k_A \gamma X_3 \\
 F_4 &= k_A \gamma X_4 \\
 F_5 &= k_A \gamma X_5 \\
 F_6 &= k_A \gamma X_6 \\
 F_7 &= k_A \gamma X_7 \\
 F_8 &= k_A \gamma X_8
 \end{aligned}
 \tag{A-4}$$

substituting equation (A-3) back into equation (A-1) yields:

$$k_A \gamma \sum_{i=1}^8 X_i^2 = M$$

or

$$k_A = \frac{M}{\gamma} \left(\frac{1}{\sum_{i=1}^8 X_i^2} \right) \tag{A-4}$$

From equation (A-2)

$$\begin{aligned}
 \sum_{i=1}^8 X_i^2 &= 2 R^2 [\sin^2 \theta + \sin^2 (\theta + 45) + \cos^2 \theta + \cos^2 (\theta + 45)] \\
 &= 4 R^2
 \end{aligned}$$

Thus:

$$k_A = \left(\frac{M}{\gamma} \right) \frac{1}{4R^2} \tag{A-5}$$

or, the bearing system bending stiffness k_B is:

$$k_B = \frac{M}{\gamma} = 4R^2 k_A \tag{A-6}$$

From equation (A-6), the joint's bending moment stiffness M/γ due to the compliance of the bearing support system alone (that is, the rotating ring is considered rigid) is independent of rotation angle, θ , and directly proportional to the individual axial stiffness of the bearing moment k_A and the square of the ring radius R .

It can be shown in general that for any number of bearing hangers, Z , greater than 2, that

$$\sum_{i=1}^Z x_i^2 = \frac{Z}{2} R^2$$

so

$$K_B = \frac{Z}{2} R^2 k_A \quad (A-7)$$

Therefore the joint's bending stiffness can be increased, if necessary, by adding more bearing hangers, Z .

It should be noted that equations (A-6) and (A-7) do not consider the axial compliance of the annular ring itself, normal to its face. However, given the compliance characteristics of the ring such as that described in reference 3, it is a straightforward matter to combine it with the compliance of the bearing support system. With a discrete bearing support system, the compliance of the ring will vary with rotation in relation to the load supports. However, as shown in reference 3, this variation is relatively small and therefore of second order importance.

Radial stiffness. - Consider the rigid ring in figure 16 to be supported by a group of radial springs attached at each of the eight bearing support hangers. If an external vertical force, Q , is applied to the ring, then the rigid ring will "move" through a vertical displacement δ_v . This vertical displacement, δ_v , will, in turn, cause a local radial displacement δ_{r1} to occur at each bearing support as follows:

$$\begin{aligned} \delta_{r1} &= \delta_v \sin \theta \\ \delta_{r2} &= \delta_v \sin (\theta + 45) \\ \delta_{r3} &= \delta_v \sin (\theta + 90) = \delta_v \cos \theta \\ \delta_{r4} &= \delta_v \sin (45 - \theta) = \delta_v \cos (\theta + 45) \\ \delta_{r5} &= \delta_v \sin \theta \\ \delta_{r6} &= \delta_v \sin (\theta + 45) \\ \delta_{r7} &= \delta_v \sin (90 - \theta) = \delta_v \cos \theta \\ \delta_{r8} &= \delta_v \sin (45 - \theta) = \delta_v \cos (\theta + 45) \end{aligned} \quad (A-8)$$

Since the ring is trapped between two identical bearing supports, (see figure 9), with equal radial stiffnesses k_R then a radial force P_i as shown in figure 16 will be generated at each bearing location as given by:

$$\begin{aligned}
 P_1 &= k_R \delta_{r1} \\
 P_2 &= k_R \delta_{r2} \\
 P_3 &= k_R \delta_{r3} \\
 P_4 &= k_R \delta_{r4} \\
 P_5 &= k_R \delta_{r5} \\
 P_6 &= k_R \delta_{r6} \\
 P_7 &= k_R \delta_{r7} \\
 P_8 &= k_R \delta_{r8}
 \end{aligned}
 \tag{R-4}$$

For equilibrium, the sum of the vertical components P_{v_i} of each of the radial forces P_i must be equal to the applied force Q or

$$Q = \sum_{i=1}^8 P_{v_i}
 \tag{A-10}$$

where

$$\begin{aligned}
 P_{v1} &= P_1 \sin \theta \\
 P_{v2} &= P_2 \sin (\theta + 45) \\
 P_{v3} &= P_3 \cos \theta \\
 P_{v4} &= P_4 \cos (\theta + 45) \\
 P_{v5} &= P_5 \sin \theta \\
 P_{v6} &= P_6 \sin (\theta + 45) \\
 P_{v7} &= P_7 \cos \theta \\
 P_{v8} &= P_8 \cos (\theta + 45)
 \end{aligned}
 \tag{A-11}$$

Substituting equations (A-8) through (A-10) into equation (A-11) yields:

$$Q = \sum_{i=1}^8 P_{v_i} = 2k_R \delta_v \left[\sin^2(\theta) + \sin^2(\theta + 45) + \cos^2\theta + \cos^2(\theta + 45) \right]$$

or

$$Q = 4k_R \delta_v$$

Thus the radial system stiffness K_R becomes:

$$K_R = \frac{Q}{\delta_v} = 4k_R \quad (A-12)$$

In general, it can be shown that for any number of bearing hangers Z that

$$K_R = \frac{Z}{2} k_R$$

APPENDIX B - CAM BEARING STIFFNESS

In the main text it was shown that minimum axial support bearing stiffness values of approximately 8.9×10^7 N/m and 2.9×10^7 N/m were needed for the 2.4 and 4.3 m (8 and 14 ft) joints respectively. It was also shown that a minimum radial stiffness of about 1.8×10^7 N/m (10^5 lb/in.) was needed for both size joints. Based on these k values a representative cam bearing size can be found.

To illustrate the stiffness integrity of the joint, select a representative cam roller bearing having the following dimensions:

o.d. = 5.08 cm
width = 3.18 cm
stud diameter = 2.86 cm
maximum static capacity - 47 000 N
basic dynamic capacity - 36 000 N
material = 440-C stainless steel

Cantilevered Beam Bending Stiffness

$$k_b = \frac{P}{\Delta} = \frac{3 EI}{l^3} \quad (B-1)$$

For

$$E = 207 \text{ GPa}, I = 3.27 \times 10^{-8} \text{ m}^4 \text{ and } l = 0.0152 \text{ m}$$

then

$$k_b = 5.79 \times 10^9 \text{ N/m (} 33.05 \times 10^6 \text{ lb/in.)}$$

Needle Roller Hertzian Stiffness, k_r

For 25 needle rollers of 0.414 cm diameter and 1.73 cm wide (see table B-1).

Cam Bearing Against Ring Track Hertzian Stiffness, k_c

According to methods of reference 20, the Hertzian stiffness of two solid elastic cylindrical bodies in direct bearing contact is given by

$$k_c = 4.018 \times 10^8 p^{0.1} l^{0.8} \quad (\text{N and m units})$$

For the steel cam roller outer race in external contact with either a steel ring track or one made from aluminum, the following stiffness values k_c can be found as a function of normal preload, P_0 .

For the steel roller outer race of width $l = 31.8$ mm in external contact with either a steel ring track or one made from aluminum, the following k_c values can be found from the above equation as a function of preload, P_0 (see table B-2).

Cam Bearing Normal Stiffness, k_n

Because of the bearing post bending, needle roller and cam/ring contact acts like springs in series, then

$$\frac{1}{k_n} = \frac{1}{k_b} + \frac{1}{k_r} + \frac{1}{k_c} \quad (B-3)$$

Thus the individual, cam bearing normal stiffness k_n variation with preload is given by table B-3.

Cam Bearing Axial and Radial Stiffness

As shown in figure 9, the proposed bearing support traps the rotating ring in a triangular support system. The taper angle, ϕ , formed by this support as illustrated in figure 17 will dictate the split between axial stiffness k_A and radial stiffness k_r . From figure 17(a) it follows that:

$$P_A = 2P \sin \phi$$

and

$$\delta_A = \frac{\delta}{\sin \phi}$$

thus

$$k_A = \frac{P_A}{\delta_A} = \frac{2P}{\delta} \sin^2 \phi = 2k_n \sin^2 \phi \quad (B-4)$$

and from figure 16(b), it follows that:

$$P_R = P \cos \phi$$

and

$$\delta_R = \frac{\delta}{\cos \phi}$$

thus

$$k_R = \frac{P_R}{\delta_R} = \frac{P}{\delta} \cos^2 \phi = k_n \cos^2 \phi \quad (B-5)$$

If $\phi = 45^\circ$, then:

$$k_A = k_n \quad (B-6)$$

and

$$k_R = \frac{k_n}{2} \quad (B-7)$$

Bearing System Axial and Radial Stiffness, K_A and K_B

Equations (B-6) and (B-7) give individual bearing axial and radial stiffness in terms of the normal stiffness k_n as tabulated in table B-3 as a function of roller/ring material and preload. System bending and radial stiffness can, therefore, be found from equations (A-6) and (A-12), respectively, in terms of k_A and k_R . These values are listed in table B-4 for joints 2.4 and 4.3 m in diameter.

Preload Selection

According to table I, a maximum transient bending moment of 4290 N-m will be imposed on the joint during shuttle berthing maneuvers. In order to sustain this berthing moment a sufficiently large axial bearing preload or clamping force must be initially imposed to prevent the cam roller from losing contact with the ring. If a constant axial preload force of F_p is imposed in each bearing hanger, it is apparent from figure 15 that

$$M = F_p \sum_{i=1}^8 x_i \quad (B-8)$$

where x_i is given by equation (A-2). Substituting equation (A-2) into equation (B-8) and simplifying yields:

$$F_p = \frac{M}{2R} [\sin \theta + \sin(\theta + 45) + \cos \theta + \cos(\theta + 45)]$$

For

$M = 4290$ N-m, maximum $F_p = 742$ N for $2R = 2.4$ m and

$$F_p = 424$$
 N for $2R = 4.3$ m (B-9)

TABLE B-1. - NEEDLE ROLLER
STIFFNESS

$k_r, 10^9 \text{ N/m}$	Bearing preload, N
1.17	445
1.26	890
1.48	4 450
1.73	22 200

TABLE B-2. - CAM/RING STIFFNESS

$k_c, 10^9 \text{ N/m}$		Preload, N
Steel roller/ steel ring	Steel roller/ aluminum ring	
7.95	4.20	445
8.16	4.50	890
9.58	5.29	4 450
11.3	6.22	22 200

TABLE B-3. - CAM BEARING NORMAL
STIFFNESS

$k_n, 10^9 \text{ N/m}$		Preload, N
Steel roller/ steel ring	Steel roller/ aluminum ring	
0.87	0.79	445
.92	.84	890
1.05	.96	4 450
1.19	1.10	22 200

TABLE B-4. - CAM BEARING SYSTEM BENDING AND RADIAL STIFFNESS

Joint diameter, m	Preload, N	Bending stiffness, $K_B, 10^9 \text{ N-m/rad}$		Radial stiffness, $K_R, 10^9 \text{ N/m}$	
		Steel roller, steel ring	Steel roller, aluminum ring	Steel roller, steel ring	Steel roller, aluminum ring
2.4	445	20.0	18.2	1.74	1.58
	890	21.2	19.4	1.84	1.68
	4 450	24.2	22.1	2.10	1.92
	22 200	27.4	25.3	2.38	2.20
4.3	445	64.4	58.4	1.74	1.58
	890	68.0	62.1	1.84	1.68
	4 450	77.7	71.0	2.10	1.92
	22 200	88.0	81.4	2.38	2.20

APPENDIX C - TRACTION ROLLER DRIVE DESIGN

The roller drive actuator must have sufficient torque with some safety margin to overcome the basic "rotating drag" of the joint and to accelerate the rotating structure up to speed in some reasonable time period.

Accelerating Torque, T_{ac}

From table I, the inertial load, $I = 6.0 \times 10^5 \text{ kg-m}^2$ for 4 photovoltaic panels of $9.2 \times 24.4 \text{ m}$ in size. If the required maximum acceleration rate α is $0.003^\circ/\text{sec}^2$ ($\approx 21 \text{ sec}$ to accelerate from rest to nominal speed $0.064^\circ/\text{sec}$)

then:

$$\begin{aligned} T_{ac} &= I\alpha && \text{(C-1)} \\ &= 31.4 \text{ N-m} \end{aligned}$$

Electrical Transfer Device

For purposes of sizing, a multicircuit roll ring as described in reference 12 will be selected for both power and data transfer. According to reference 12, a 200 amp, 10 flexure roll ring will have a drag torque per circuit of $3.5 \times 10^{-3} \text{ N-m}$. If 16 circuits are selected for power (4 per panel) and 16 circuits for data then the total drag torque for the roll-ring $T_{RR} = 32 \times 3.5 \times 10^{-3} \text{ N-m} = 0.11 \text{ N-m}$. Let $T_{RR} = 1 \text{ N-m}$ for conservatism.

Cam Bearing Drag Torque, T_{CB}

Typical cam roller bearings have a friction coefficient $f = 0.002$. For 24 cam bearings (eight hangers by three bearings/hanger) preloaded to 1000 N (742 N minimum) for the 2.4 m joint and to 500 N (424 N minimum) for the 4.3 m joint then:

$$\begin{aligned} T_{CB} &= 24 f F_p R \\ &= 24(0.002)(1000)(1.2) \\ &= 57.6 \text{ N-m} && \text{For the 2.4 m joint} \\ &= 24(0.002)(500)(2.15) \\ &= 51.6 \text{ N-m} && \text{For the 4.3 m joint} \end{aligned}$$

Roller Contact Torque Loss

Assuming a minimum torque transfer efficiency of 90 percent, the roller torque loss:

$$\begin{aligned} T_{RL} &= 0.1 (T_{ac} + T_{RR} + T_{CB}) && \text{(C-3)} \\ &= 9 \text{ N-m} && \text{For 2.4 m joint} \\ &= 8.4 \text{ N-m} && \text{For 4.3 m joint} \end{aligned}$$

If a safety factor of 2 is applied to the rolling ring cam bearing and roller contact loss torques, then the total system output torque is obtained as follows:

$$\begin{aligned} T_o &= T_{AC} + 2 \times (T_{RR} + T_{CB} + T_{RL}) \\ &= 166.6 \text{ N-m} && \text{For 2.4 m joint} \\ &= 153.4 \text{ N-m} && \text{For 4.3 m joint} \end{aligned}$$

For the "pinch" roller pair (see fig. 7), the traction force F_T per roller is given by

$$F_T = \frac{1}{2} \frac{T_o}{R} \quad (C-5)$$

The normal load N is dependent on the design traction coefficient, μ , according to

$$N = \frac{F_T}{\mu} = \frac{1}{2} \frac{T_o}{R\mu} \quad (C-6)$$

and the maximum Hertzian stress, S_{max} , in line contact for a drive roller of width W is given by:

$$S_{max} = \left[\pi \left(\frac{1 - \nu_a^2}{E_a} + \frac{1 - \nu_b^2}{E_b} \right) \right]^{-1/2} \left[\frac{P}{W} \left(\frac{1}{R_b} - \frac{1}{R_a} \right) \right]^{1/2} \quad (C-7)$$

where ν is Poisson's ratio, E is the elastic modulus and subscripts a and b denote the ring and roller material, respectively.

The effect of joint diameter, drive roller diameter and design traction coefficient on drive roller normal load, unit normal load and maximum Hertz stress based on equations (C-2) through (C-7) is summarized in table C-1. The roller width to diameter ratio, $W/2R_b$, is set at 1.5. The results are based on a "pinch" roller drive pair as shown in figure 7.

TABLE C-1. - DRIVE ROLLER LOADING SUMMARY

Traction coefficient, μ	Ring radius, R_a , m	Roller radius, R_b , m	Normal load, Q , N	Unit ^b , Normal load, Q/W , N/m	Maximum Hertz stress, S_{max} , 10^6 N/m ² , Ring/roller material		
					Steel/steel	Aluminum/steel	Aluminum/polyimide
0.1	1.2	0.025	694	9260	117.0	88.5	18.4
		.038	694	6170	78.4	59.3	12.3
		.050	694	4630	59.1	44.7	9.3
	2.15	.025	357	4760	83.5	63.1	13.1
		.038	357	3170	55.4	42.2	8.8
		.050	357	2380	41.8	31.8	6.6
.2	1.2	.025	347	4630	82.7	62.6	13.0
		.038	347	3090	55.4	41.9	8.7
		.050	347	2310	41.8	31.6	6.6
	2.15	.025	178	2380	59.0	44.6	9.3
		.038	178	1590	39.5	29.8	6.2
		.050	178	1190	29.7	22.4	4.7
.3	1.2	.025	231	3090	67.5	51.1	10.6
		.038	231	2060	45.3	34.2	7.1
		.050	231	1540	34.1	25.8	5.4
	2.15	.025	119	1590	48.2	36.4	7.6
		.038	119	1060	32.2	24.4	5.1
		.050	119	793	24.2	18.3	3.8

^aOutput torque, $T_0 = 166.6$ N-m for $R_a = 1.2$ m.
 $= 153.4$ N-m for $R_a = 2.15$ m.

^bWidth/diameter = $W/2R_b = 1.5$.

REFERENCES

1. Space Station Reference Configuration Description. NASA TM-87493, (JSC-19989) 1984.
2. Mikulas, M.M., Jr. et al.: Deployable-Erectable Trade Study for Space Station Truss Structures, NASA TM-87573, 1985.
3. Lake, M.S.; and Bush, H.G.: An Analytical Investigation of a Conceptual Design for the Space Station Transverse Boom Rotary Joint Structure, NASA TM-87665, 1986.
4. Loewenthal, S.H.: Roller Drive Rotary Joint Advanced Development Program. Program Review presented for the NASA Mechanisms Technical Integration Panel, NASA Johnson Space Center, June 12, 1985.
5. Loewenthal, S.; Rohn, D.; and Steinetz, B.: Application of Traction Drives as Servo Mechanisms. Nineteenth Aerospace Mechanisms Symposium, NASA CP-2371, 1985, pp. 119-139.
6. Loewenthal, S.H.; Rohn, D.A.; and Anderson, N.E.: Advances in Traction Drive Technology. SAE Paper 831304, Sept. 1983.
7. Bryan, J.B.: Design and Construction of an Ultraprecision 84 Inch Diamond Turning Machine, Prec. Eng., vol. 1, no. 1, Jan. 1979, pp. 13-17.
8. Smith, L.T.: Commonality of Solar Array/Radiator/Platform Gimbals, McDonnell Douglas Mechanisms Technical Integration Panel Presentation at NASA Marshall Space Flight Center, July 30, 1985.
9. Mueller, J.W.: The Helios Experiment 5 Antenna Mechanism. 10th Aerospace Mechanisms Symposium, NASA CR-148515, (JPL-TM-33-777) 1976, pp. 133-142.
10. Smith, G.A.: Metal With a Memory Provides Useful Tool For Skylab Astronauts. 9th Aerospace Mechanisms Symposium, NASA TM X-3274, 1975, pp. 81-97.
11. Rowntree, R.A.: The Properties of Thin-Section, Four-Point-Contact Ball Bearings in Space. Nineteenth Aerospace Mechanisms Symposium, NASA CP-2371, 1985, pp. 141-166.
12. Porter, R.S.: A Rotating Electrical Transfer Device. Nineteenth Aerospace Mechanisms Symposium, NASA CP-2371, 1985, pp. 277-291.
13. Gupta, P.K.; and Walowit, J.A.: Contact Stresses Between an Elastic Cylinder and a Layered Elastic Solid. J. Lubr. Technol., vol. 96, no. 2, Apr. 1974, pp. 250-257.
14. Rittenhouse, J.B.; and Singletary, J.B.: Space Materials Handbook, 3rd ed., NASA SP-3051, 1969.
15. Steinetz, B.M.; Rohn, D.A.; and Anderson, W.J. Evaluation of a High Torque Backlash-Free Roller Actuator. Twentieth Aerospace Mechanisms Symposium, NASA CP-2423, 1986, pp. 215-240.

16. Stevens, K.T.: The Tribology of Gears for Satellite Applications. First European Space Mechanisms and Tribology Symposium, ESA SP-196, T.D. Guyenne and J.J. Hunt, eds., European Space Agency, 1983, pp. 131-145.
17. Tevaarwerk, J.L.: Rolling, Slip, and Endurance Traction Measurements on Low Modulus Materials. (IR-3, Transmission Research Inc.; NASA Contract DEN3-35) NASA CR-174909, 1985.
18. Fusaro, R.L.; and Hady, W.F.: Low Wear Partially Fluorinated Polyimides. ASLE Trans., vol. 28, no. 4, Oct. 1985, pp. 542-550.
19. Fusaro, R.L.: Private Communication, 1986.
20. Palmgren, A.: Ball and Roller Bearing Engineering, 3rd ed., SKF Industries, Inc., Philadelphia, PA, 1959.

TABLE I. - ALPHA ROTARY JOINT DRIVE OPERATING DESIGN REQUIREMENTS

Travel, deg/sec	360
Maximum slew rate, deg/sec	0.5
Nominal slew rate, deg/sec, min/rev	0.064 (94)
Maximum acceleration rate, deg/sec ²	0.003
Position accuracy, deg	±1
Maximum shuttle berthing load, in.-lb/rad	4290 (38 000) bending
Transient response to 2224 N step load for 1 sec	3390 (30 000) torsion
Launch load	TBD
Bending stiffness N-m/rad, in.-lb/rad ^a	5.31x10 ⁸ (4.7x10 ⁹)
Torsional stiffness N-m/rad, in.-lb/rad ^a	1.43x10 ⁸ (1.27x10 ⁹)
Inertia load, Kg-m ² , slug-ft ²	6.0x10 ⁵ (4.4x10 ⁵)
Design life, years, joint revs ^a	10 (55 900)
Temperatures, °C, °F	-54 to 121 (-65 to 250) without insulation
Absolute pressure at 250 N.MI, torr	1.3x10 ⁻⁶ to 2.46x10 ⁻⁴

^aFrom reference 8.

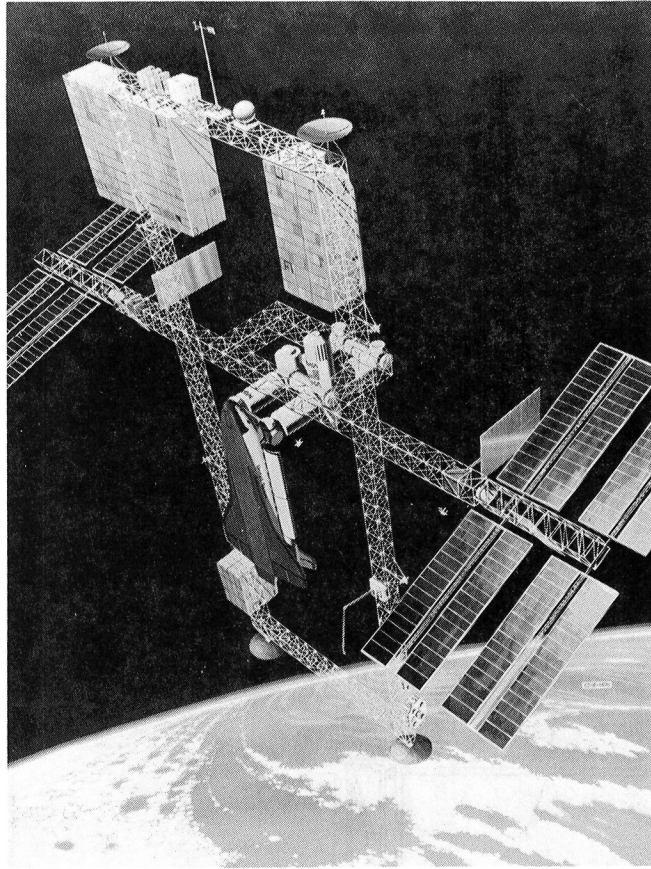


Figure 1. - Dual keel photovoltaic powered space station

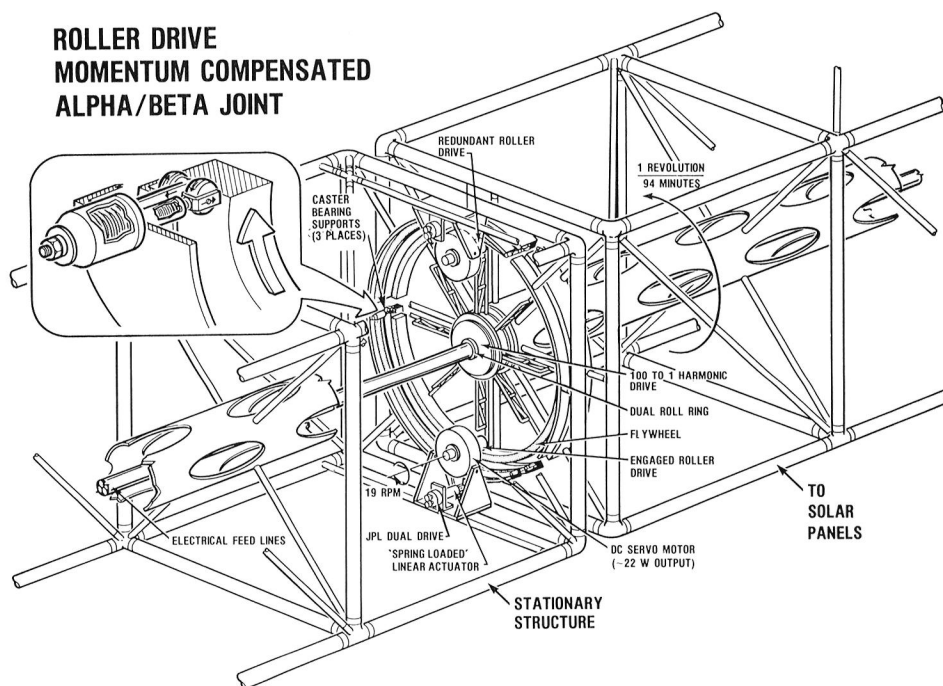


FIGURE 2. - ROLLER/WHEEL ROTARY JOINT CONCEPT.

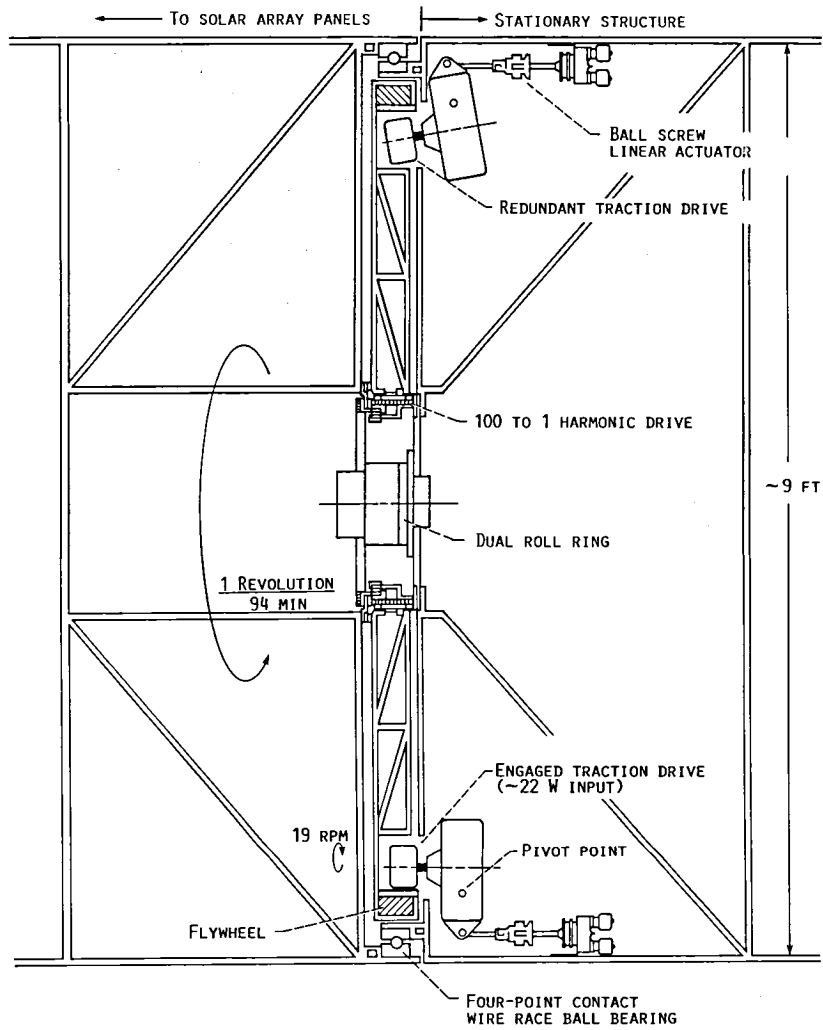


FIGURE 3. - CROSS-SECTION OF ROLLER/WHEEL CONCEPT SHOWING DETAILS OF LINEAR ACTUATOR SYSTEM.

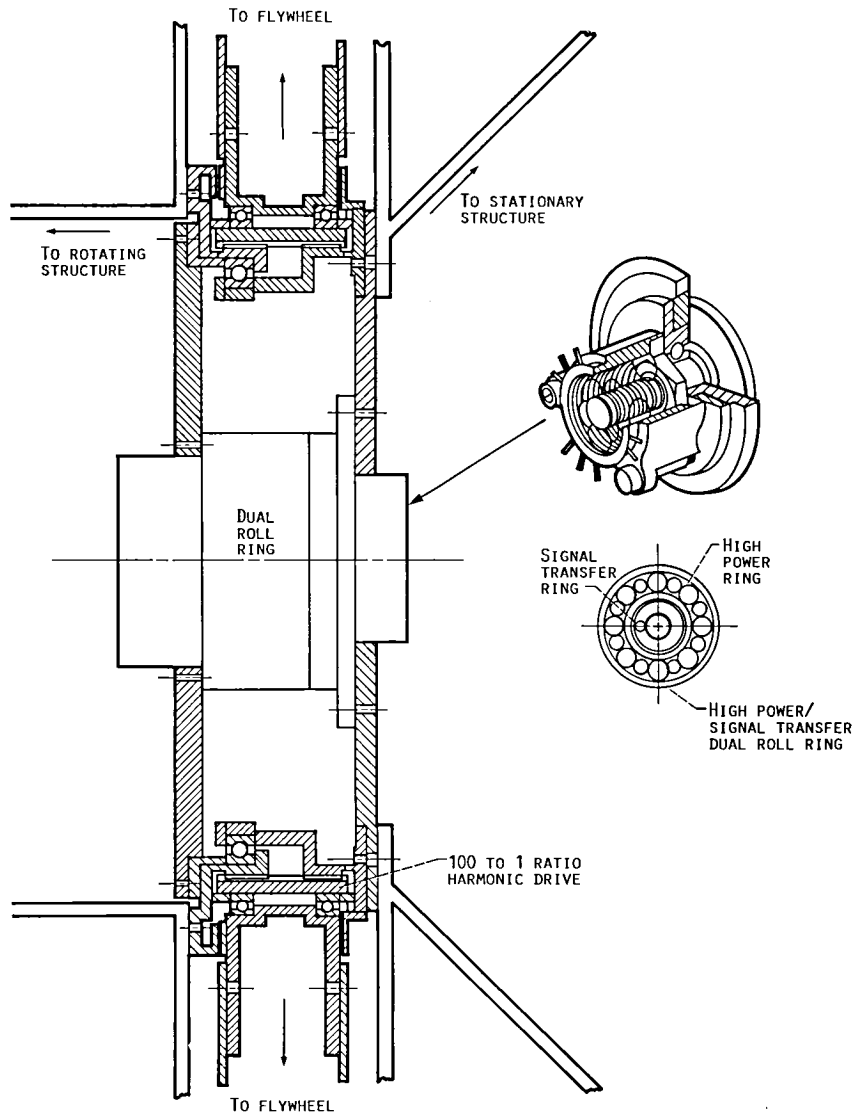


FIGURE 4. - DETAILS OF HARMONIC DRIVE AND ROLL RING.

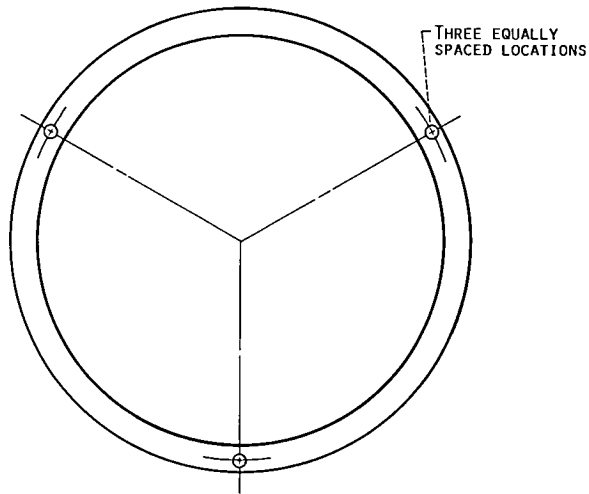
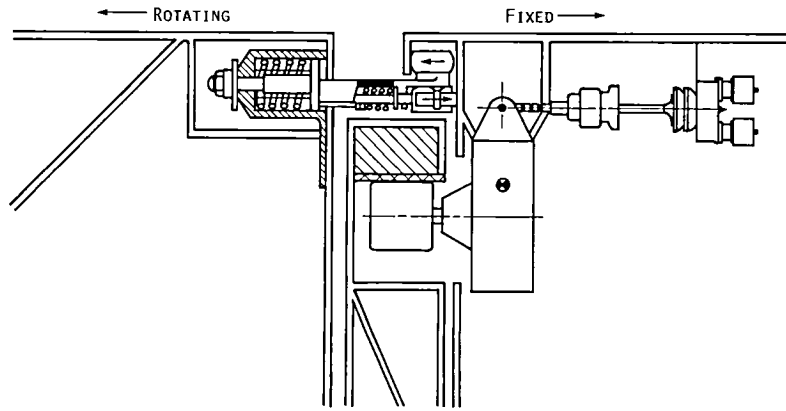


FIGURE 5. - CASTER BEARING SUPPORT SYSTEM.

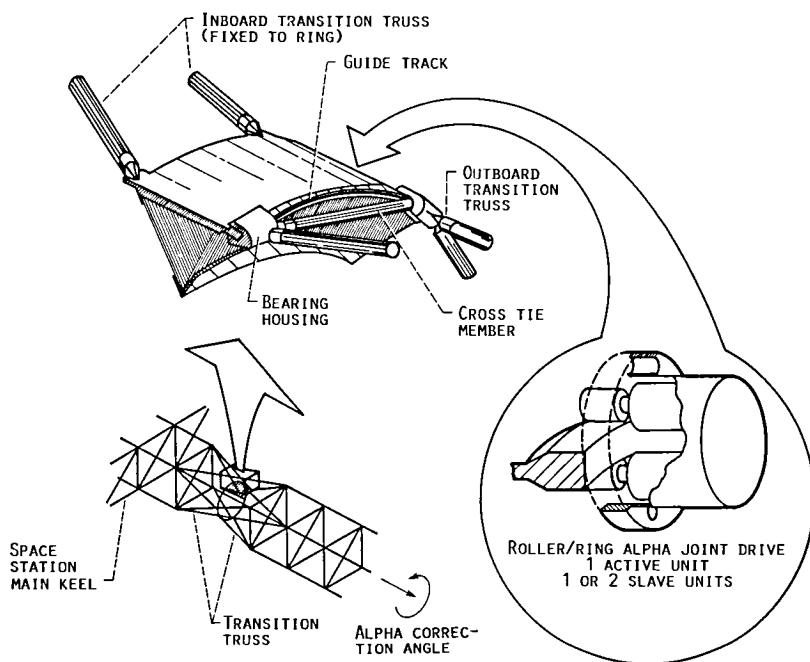


FIGURE 6. - DISCRETE BEARING/DIRECT ROLLER DRIVE ROTARY JOINT CONCEPT.

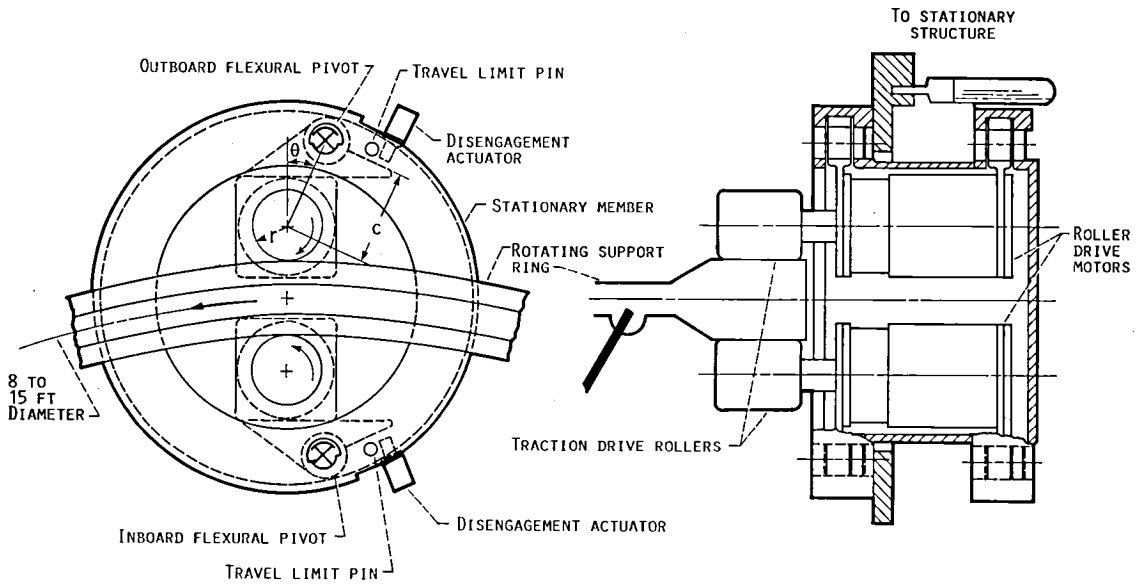


FIGURE 7. - DETAILS OF SELF-LOADING PINCH ROLLER DRIVE MECHANISM.

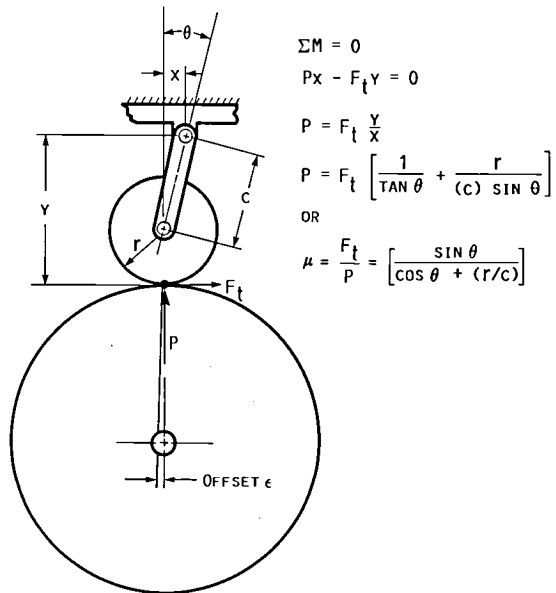


FIGURE 8. - SELF-LOADING ROLLER DRIVE GEOMETRY.

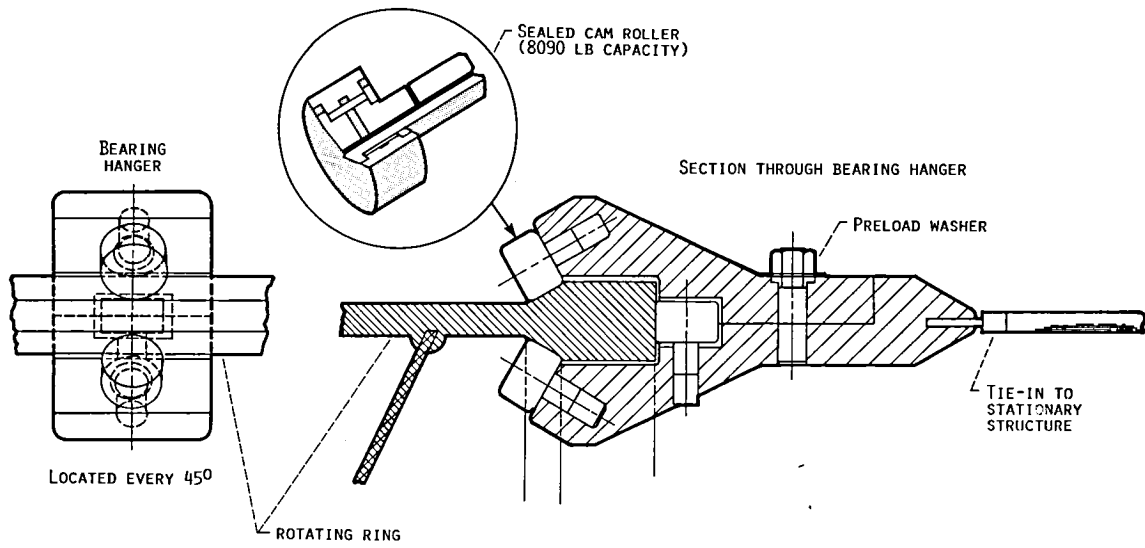


FIGURE 9. - DETAILS OF CAM BEARING SUPPORT HANGER ASSEMBLY.

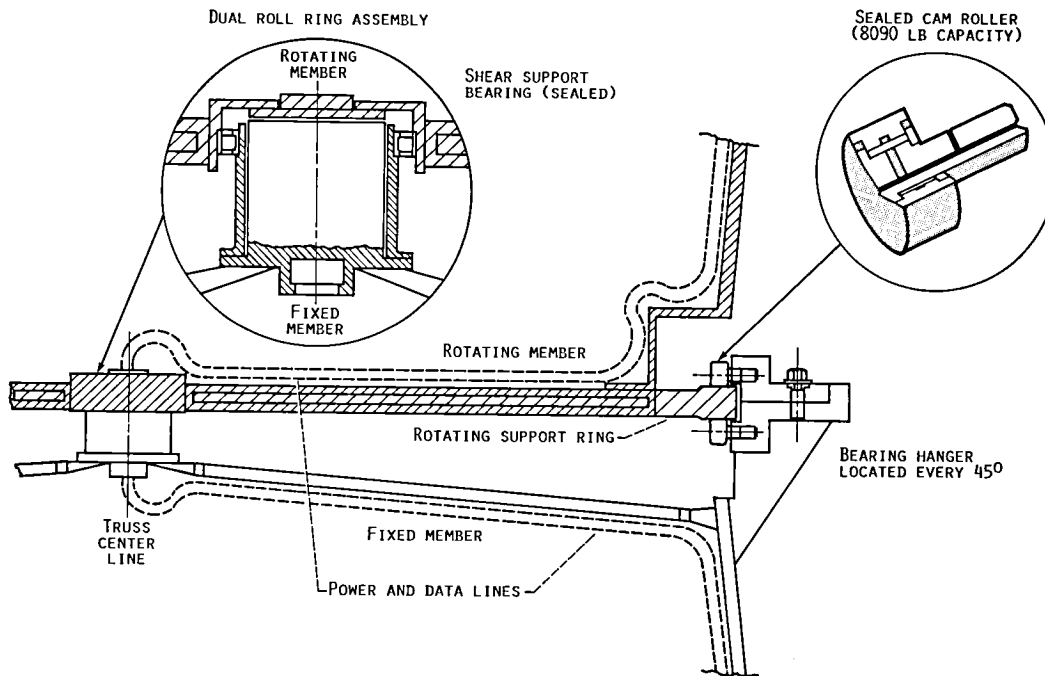


FIGURE 10. - ALTERNATE CAM BEARING SUPPORT SHOWING DECOUPLING OF MOMENT AND SHEAR LOAD SUPPORT FUNCTIONS.

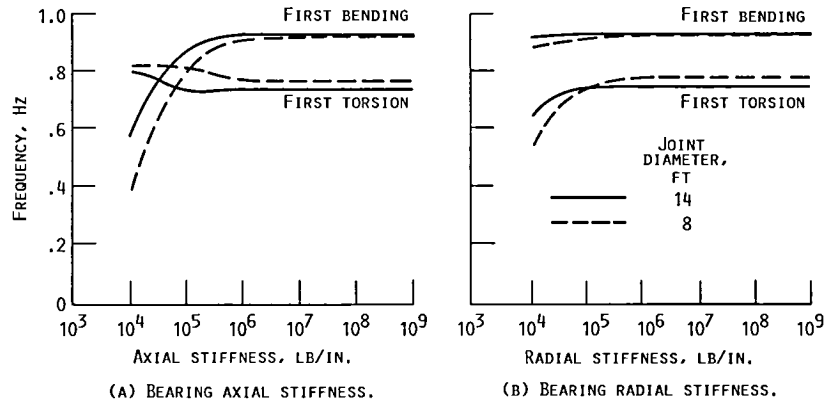


FIGURE 11. - EFFECT OF BEARING MOUNT STIFFNESS ON SOLAR WING FUNDAMENTAL FREQUENCIES FROM REFERENCE 3.

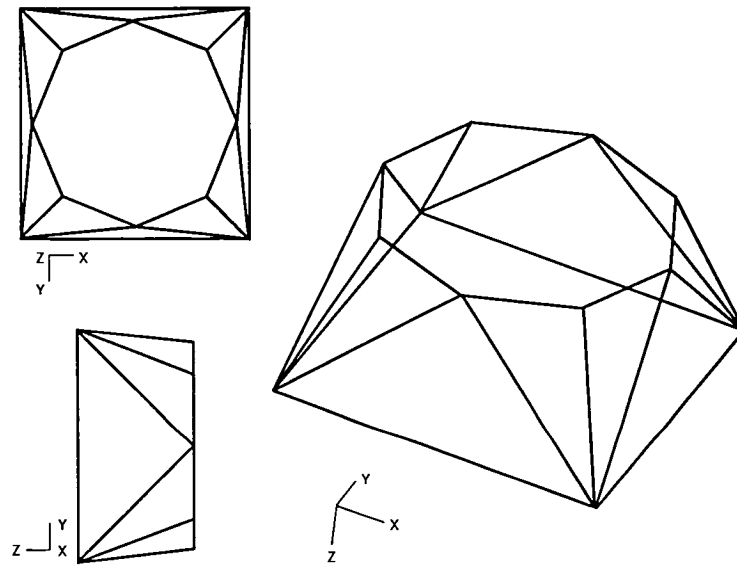
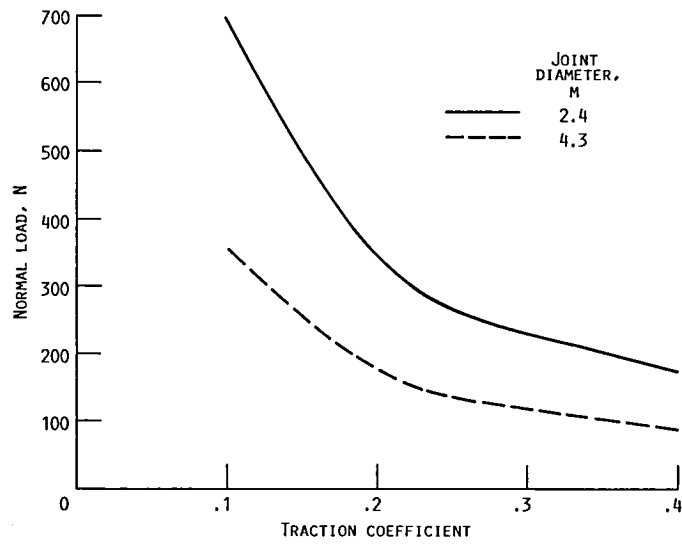
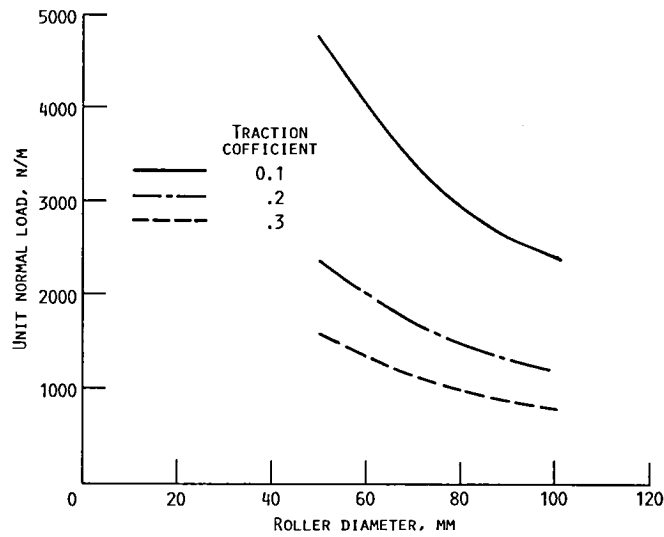


FIGURE 12. - NASTRAN MODEL OF TRANSITION TRUSS STRUCTURE.

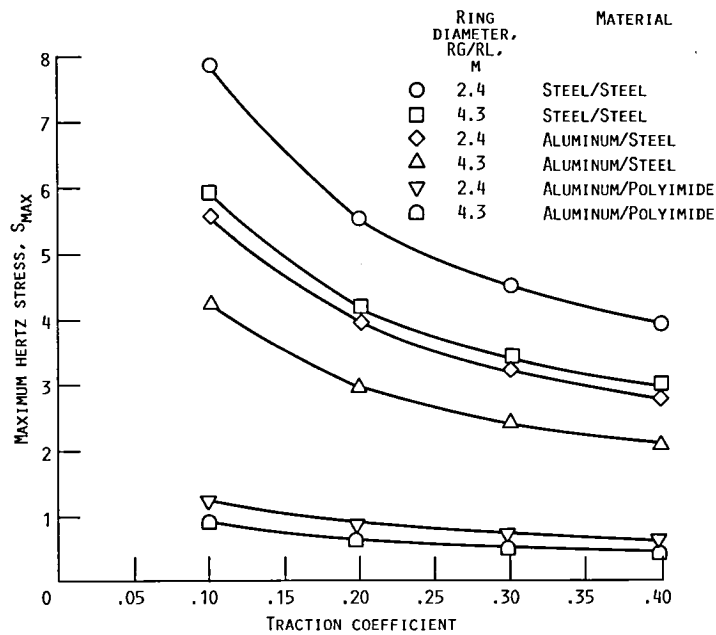


(A) EFFECT OF TRACTION COEFFICIENT ON NORMAL LOAD.



(B) EFFECT OF ROLLER DIAMETER ON UNIT NORMAL LOAD. ROLLER WIDTH/DIAMETER = 1.5; JOINT DIAMETER = 4.3 M.

FIGURE 13. - EFFECT OF TRACTION COEFFICIENT, ROLLER/JOINT DIAMETER AND MATERIALS ON ROLLER CONTACT LOADING AND STRESS. ROLLER WIDTH/DIAMETER = 1.5.



(C) EFFECT OF TRACTION COEFFICIENT AND MATERIAL ON MAXIMUM HERTZ STRESS. ROLLER DIAMETER = 75 MM; ROLLER WIDTH = 113 MM.

FIGURE 13. - CONCLUDED.

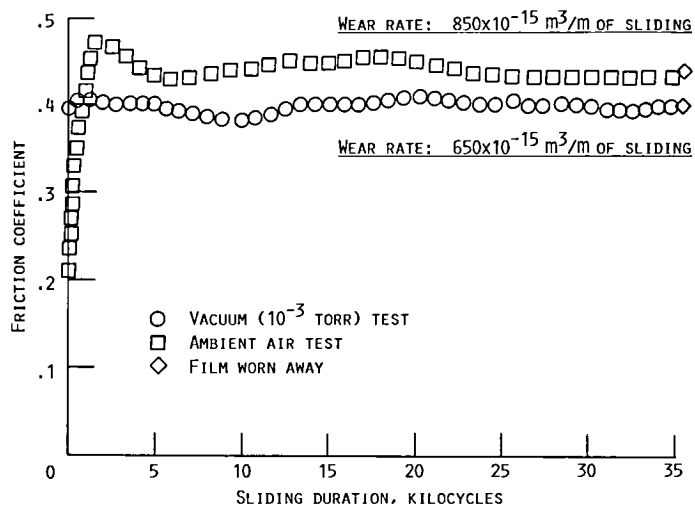


FIGURE 14. - COMPARISON OF FRICTION AND WEAR CHARACTERISTICS OF AN EXPERIMENTAL PARTIALLY FLUORINATED POLYIMIDE FILM IN AIR AND VACUUM (REF. 19) PIN ON DISK TEST DATA. (FILM THICKNESS = 25 TO 50 μm ; SLIDING SPEED = 0.31 M/S; NORMAL LOAD = 1 KG; ROTATIONAL SPEED = 100 RPM; AISI 440-C STEEL PIN OF 0.95 CM DIAMETER AGAINST POLYIMIDE COATED STEEL DISK.)

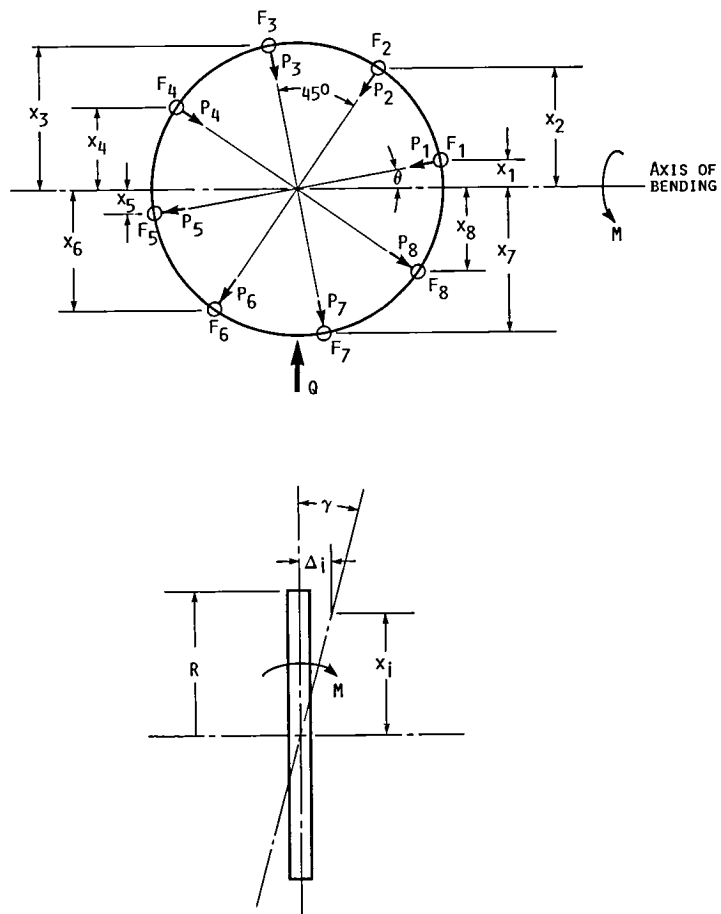


FIGURE 15. - BEARING SUPPORT SYSTEM STIFFNESS PARAMETERS.

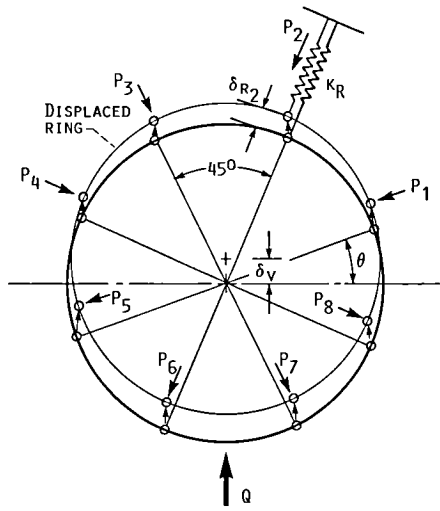
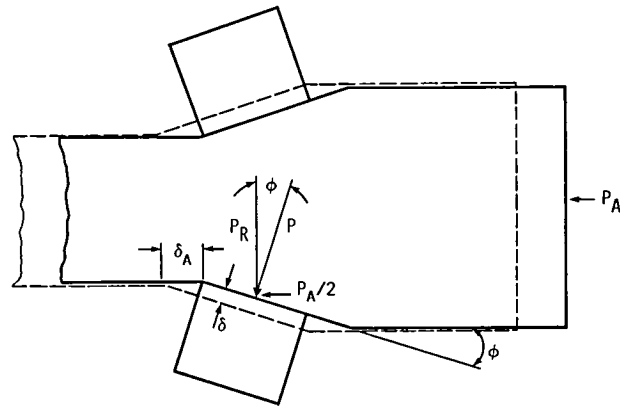
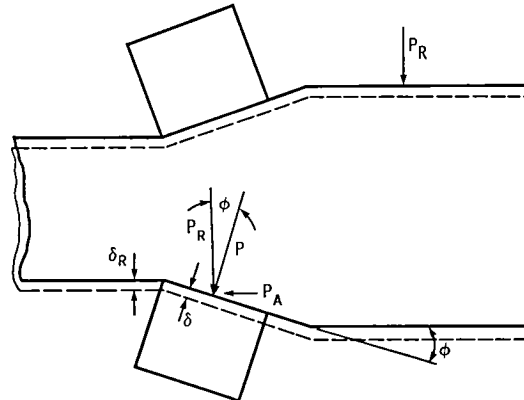


FIGURE 16. - BEARING SYSTEM RADIAL STIFFNESS (RING VERTICALLY DISPLACED δ_v BY FORCE Q).



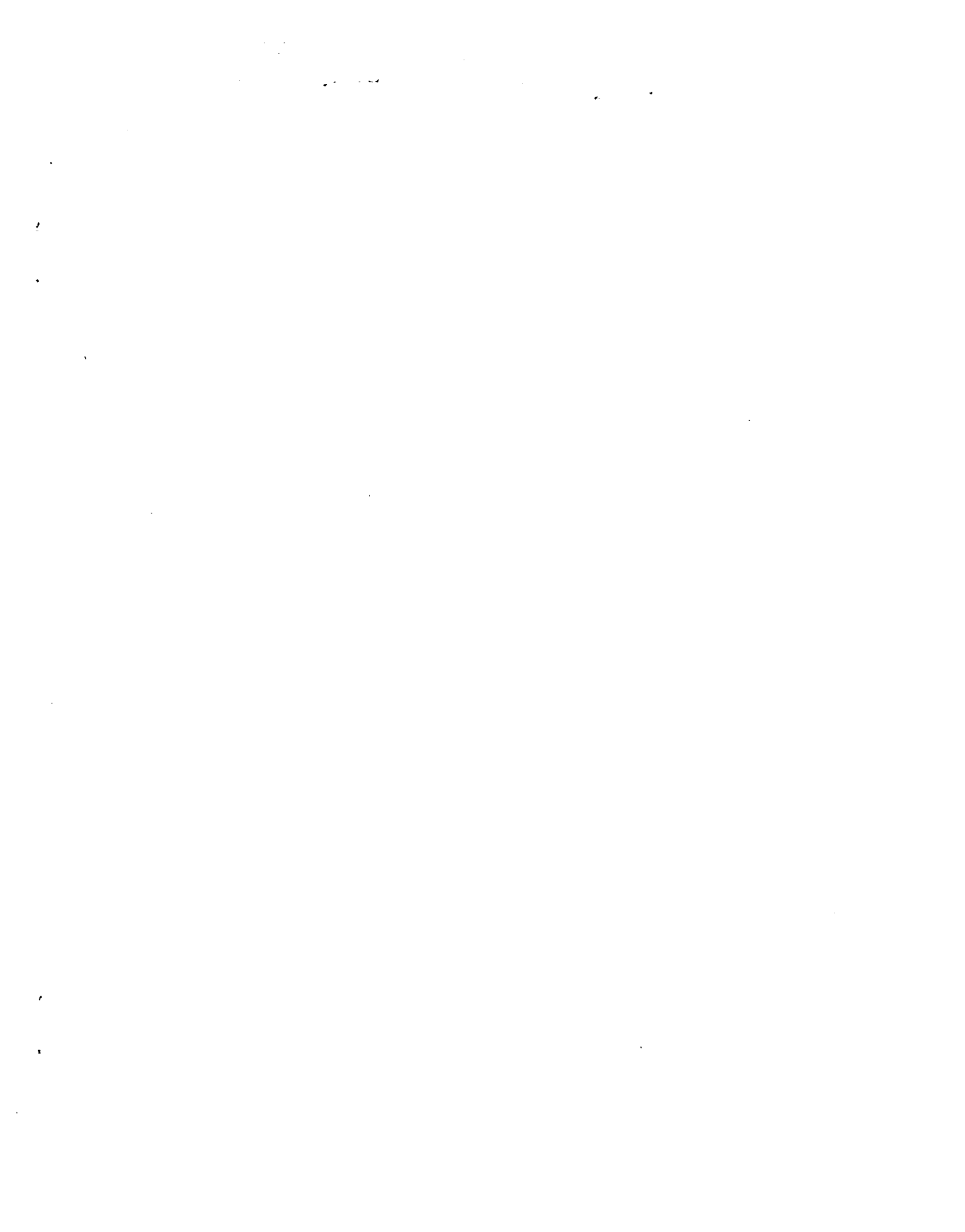
(A) AXIAL.



(B) RADIAL.

FIGURE 17. - FORCES AND DEFLECTIONS FOR STIFFNESS CALCULATIONS.

1. Report No. NASA TM-88800		2. Government Accession No.		3. Recipient's Catalog No.	
4. Title and Subtitle Feasibility Study of a Discrete Bearing/Roller Drive Rotary Joint for the Space Station				5. Report Date July 1986	
				6. Performing Organization Code 505-63-11	
7. Author(s) Stuart H. Loewenthal and Fredrick T. Schuller				8. Performing Organization Report No. E-3138	
9. Performing Organization Name and Address National Aeronautics and Space Administration Lewis Research Center Cleveland, Ohio 44135				10. Work Unit No.	
				11. Contract or Grant No.	
12. Sponsoring Agency Name and Address National Aeronautics and Space Administration Washington, D.C. 20546				13. Type of Report and Period Covered Technical Memorandum	
				14. Sponsoring Agency Code	
15. Supplementary Notes					
16. Abstract Perhaps the most critical mechanism on board the proposed space station is the continuously rotating joint which must accurately align the solar power units with the sun during earth orbit. The feasibility of a multiple, discrete bearing supported joint driven by a self-loading, "pinch" roller drive actuator was investigated for this application. This concept appears to offer greater protection against catastrophic jamming, less sensitivity to adverse thermal gradients, greater accessibility to inorbit servicing or replacement and greater adaptability to very large (5 m) truss members than to more conventional continuous support bearing/gear reducer joints. Analytical trade studies performed herein establish that a discrete cam roller bearing support system having eight hangers around a continuous ring would provide sufficient radial and bending stiffness to prevent any degradation in the fundamental frequencies of the solar wing structure. Furthermore, it appears that the pinch roller drive mechanism can be readily sized to meet or exceed system performance and service life requirements. Wear life estimates based on experimental data for a steel roller coated with an advanced polyimide film show a continuous service life more than two orders of magnitude greater than required for this application.					
17. Key Words (Suggested by Author(s)) Rotary joint; Transverse boom; Discrete bearing; Space station mechanism; Traction drive			18. Distribution Statement Unclassified - unlimited STAR Category 37		
19. Security Classif. (of this report) Unclassified		20. Security Classif. (of this page) Unclassified		21. No. of pages	22. Price*



National Aeronautics and
Space Administration

Lewis Research Center
Cleveland, Ohio 44135

Official Business
Penalty for Private Use \$300

SECOND CLASS MAIL

ADDRESS CORRECTION REQUESTED



Postage and Fees Paid
National Aeronautics and
Space Administration
NASA-451

NASA
